Macromolecules
COMMUNICATION TO THE EDITOR

Macromolecules **2009**, *42*, 7627–7630 **7627**
DOI: 10.1021/ma901361s

Novel Design Solving the Conductivity vs Water-Uptake Trade-Off for Polymer Electrolyte Membrane by Bicontinuous Crystalline/Amorphous Morphology of Block Copolymer

Hiroki Uehara,*,† Masaki Kakiage,†,§,⊥ Miho Sekiya,† Tsukasa Yamagishi,† Takeshi Yamanobe,† Katsuhiko Nakajima,‡ Toshio Watanabe,‡ Kumiko Nomura,‡ Kohei Hase,‡ and Masatoshi Matsuda‡

†*Department of Chemistry and Chemical Biology, Gunma University, Kiryu, Gunma 376-8515, Japan, and* ‡*Material Engineering Division, Toyota Motor Corp., Toyota, Aichi 471-8572, Japan.* §*Research Fellow of the Japan Society for the Promotion of Science.* ⊥*Present address: Department of Applied Chemistry, Saitama University.*

Received June 25, 2009
Revised Manuscript Received September 18, 2009

Fuel cells have the great advantage of not producing carbon dioxide and thus are expected to become ideal electric power sources worldwide.[1−3] Various polymeric materials have been applied as the electrolyte membrane for fuel cells.[4−7] The most popular are fluoropolymers, such as Nafion.[8−12] One of the characteristic features of such fluoropolymer electrolytes is their self-assembling structures under wet conditions. A preferred distribution of sulfonic acid groups in the molecular chain produces a network formation of water-cluster channels surrounded by hydrophilic acid groups that develop within the hydrophobic matrix.[6,8−11] Protons can travel through such water-cluster channels via a diffusion mechanism.[12] In this case, efficient proton conductivity necessarily requires a high water uptake of around 30 wt % because the channel width is maintained by the exclusion volume of the water cluster itself. However, the inevitable vibration causes liquid water contained in a fuel cell to leak, especially in transport applications such as automobiles, making it difficult to strictly control water content. From these viewpoints, it is highly desirable for fuel cells to operate with even lower water content.

In this study, we tried to design a new approach solving the limiting trade-off of conductivity vs water uptake for conventional polymer electrolyte membranes. We focused on a block copolymer (BCP) composed of hydrophobic and hydrophilic blocks linked within a molecular chain because the former matrix is expected to function as a backbone frame that restricts the water swelling. BCP self-assembly produces various microphase separations of different block components of nanometer size, depending on the block composition.[13,14] A crystalline block is preferable as a solid backbone. Several groups have investigated the preparation of BCPs containing crystalline blocks and their crystallization behaviors. A pioneer study by Thomas et al.[15] investigated the solution crystallization of polyethylene-*block*-polystyrene (PE-*b*-PS) with a nanoperiodic phase arrangement on the substrate. Müller et al.[16−18] reported usual crystallization from the melt for a series of PE-*b*-PS having different block compositions. In contrast, Hillmyer et al.[18,19] successfully synthesized PE-*b*-poly(lactic acid) (PLA). Register et al.[20] also prepared the double crystalline BCP composed of PE and polynorbornene and reported its unique crystallization behavior. Recently, Lodge et al.[21] developed PE-*b*-poly(ethylene-*alt*-propylene) as a precursor of nanoporous ceramic materials.

In this study, the above crystalline PE was selected as the hydrophobic matrix for the targeted BCP. PE has the simplest chain architecture but exhibits excellent chemical resistance and mechanical properties. PS was selected as the amorphous counter block, since its phenyl groups can be sulfonated by acid treatment, yielding hydrophilic poly(styrenesulfonic acid) (PSS), which is well-known as a common electrolyte polymer for fuel-cell applications.[4−6] Recently, we[22−24] found that nanoporous membranes can be prepared by selective chemical etching of PE-*b*-PS precursor films. Here, the same starting material was used, with number-average molecular weights (MWs) of 6.7×10^4 for PE and 5.4×10^4 for PS blocks. A series of films were prepared under different crystallization conditions. The detailed preparation procedure is described in the Supporting Information. Transmission electron microscopy (TEM) observation revealed the gradual connection of a cylindrical crystalline network with isothermal crystallization at 90 °C from the melt at 180 °C (see Supporting Information, Figure S1). Differential scanning calorimetry (DSC) measurements also provided the growth of a melting endotherm area with crystallization time, indicating the growth of crystalline components (Figure S2). In contrast, the shorter crystallization time limited the continuity of the crystalline components.

This continuity of the cylindrical crystalline component was confirmed using three-dimensional (3-D) imaging enabled by a grid rotation during TEM observation. A series of images were recorded at each grid angle on a CCD camera. The duplicated animation was reconstructed into the 3-D geometry of the phase arrangement via image processing that emphasizes the crystalline components (Supplementary Movie S1). Figure 1 presents the 3-D images obtained at six rotation angles for a sample film isothermally crystallized at 90 °C for 12 h. The network connections of the crystalline PE cylinders are clearly seen. The bottom set of images with higher rotation angles reveals that the crystalline network extends both laterally and perpendicularly to the microtomed plane, indicating an isotropic arrangement of crystalline networks within the sample film. Conversely, the counter amorphous PS components, corresponding to vacant spaces in Figure 1, also extend with a 3-D network connection. These morphological observations suggest that the longer crystallization yields a preferable "bicontinuous" network structure, where crystalline PE and amorphous PS components are interconnected.

We considered that selective sulfonation of PS components within such bicontinuous morphologies would produce the interconnected PSS channels supported by a crystalline PE network, which is an ideal design for an electrolyte membrane with less water swelling but effective proton conductivity. The membrane strips were sulfonated by chlorosulfonic acid,[25,26] followed by washing with chloroform, acetone, and deionized water. The detailed treatment conditions are described in the Supporting Information. Table 1 summarizes the electrolyte properties obtained for the resultant sulfonated membrane. For these electrolyte property measurements, the membrane was immersed in deionized water at room temperature for 24 h, ensuring a fully swollen state, and its weight was measured. The fully swollen membrane was immediately set with a specially designed cell with a pair of diagonally arranged electrodes (Figure S3) and

*Corresponding author. E-mail: uehara@chem-bio.gunma-u.ac.jp.

Published on Web 09/30/2009

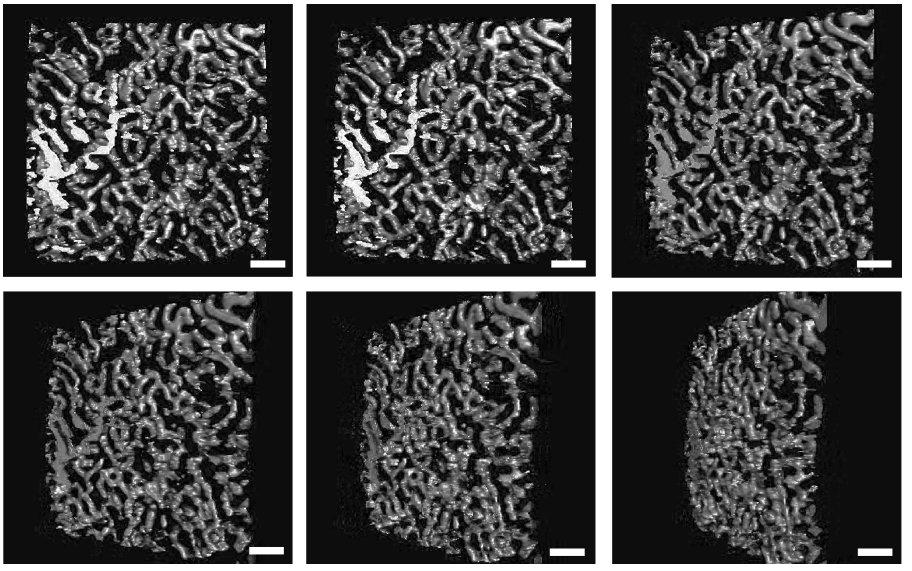

Figure 1. 3-D geometry of the crystalline morphology emphasized by the image processing of the original PE-*b*-PS film isothermally crystallized at 90 °C for 12 h. The scale bar is 100 nm. Six typical views at different rotation angles were extracted from Movie S1 and compared to determine the phase continuities.

Table 1. Electrolyte Properties for the Sulfonated Membranes Prepared in This Study[a]

run	σ^b (S/cm)	water uptake (wt %)	sulfonation degree[c] (%)	no. of trapped water molecules per sulfonic acid[d]
first	0.086	6.5	110	1.1
second	0.081	7.7	109	1.3
third	0.076	15.8	109	2.7
Nafion	0.096	34.5		10−20[e]

[a] For comparison, data for Nafion NRE211CS are provided. [b] Proton conductivity measured at 50 °C and 90% humidity after equilibrating for 1 h. [c] Estimated from the weight change measured before and after sulfonation in the dried states. [d] Calculated from the observed water uptake, assuming 100% sulfonation of PS components. [e] References 8 and 39.

equilibrated at 50 °C and 90% humidity for 1 h, followed by ac impedance recording. The membrane was then dried in a vacuum at 25−60 °C for 24 h and weighed again. The water uptake was evaluated from the weight change between the initial fully swollen state and the subsequent dried state. The detailed procedures for the electrolyte property measurements are described in the Supporting Information.

The achievable proton conductivity (σ) and water uptake were 0.086S/cm and 6.5 wt %. The obtained proton conductivity is comparable to that of the Nafion membrane, but the water uptake is much lower, corresponding to one-fifth. These values indicate the ease of water control even with high proton conductivity, which is an ideal characteristic for polymer electrolyte membranes. Here, the degrees of sulfonation estimated from the weight changes were always around 100%. A total sulfur analyzer (TSA) measurement of the sulfonated membrane indicates 90% sulfonation (Table S1), which agrees well with that obtained from the above weight change. These results suggest that one sulfonic acid group is introduced into each phenyl group of the PS component.

Such chemical structural change was also confirmed by ^{13}C-CPMAS NMR. Figure 2 compares the spectrum for the original PE-*b*-PS film and the sulfonated membrane. The spectrum of pure PSS is also included for comparison. Crystalline and amorphous methylene peaks of the PE block are located at 33 and 31 ppm.[27,28] The peaks at 41 ppm (44 ppm) is assigned to CH (CH_2) contained in PS main chain carbons. Their

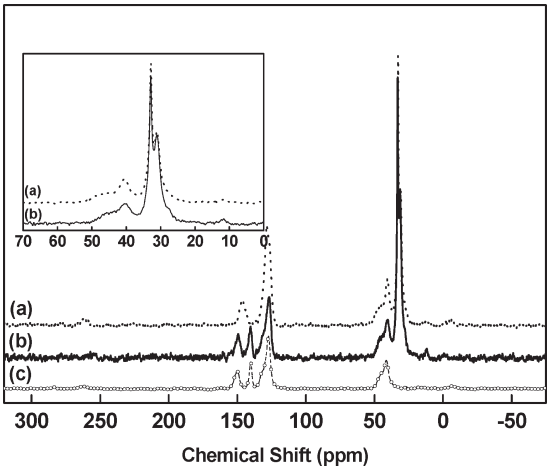

Figure 2. ^{13}C-CPMAS NMR spectrum for the original (a) and sulfonated (b) PE-*b*-PS films and for pure PSS (c). Isothermal crystallization for original film preparation was conducted at 90 °C for 3 days in a vacuum oven. The sulfonating treatment was performed in 1,2-dichloroethane at room temperature for 20 h. The inset figure enlarges the methylene backbone region from 70 to 0 ppm.

intensities and chemical shifts are unchanged even after sulfonating treatment, meaning that the methylene chain structures for both PE and PS blocks are maintained. In Figure 2a, peaks for the aromatic carbons of PS appear at 146 and 128 ppm and are respectively assigned to the quaternary carbon and CH. For PSS (Figure 2c), three peaks appearing at 150, 140, and 127 ppm are respectively assigned to quaternary carbons connected to the sulfonic acid group, the main chain, and CH. Comparing the spectrum of the sample film after sulfonating treatment (Figure 2b) with these spectra, the characteristic peak for PS at 146 ppm has completely disappeared, and Figure 2b is almost the same as Figure 2c. These results reveal that a perfect conversion into PSS could be achieved using a sulfonating treatment as performed in this study.

The thermal stability of the electrolyte membrane prepared in this study was also evaluated by DSC measurements (Figure S4a). The heat of fusion was slightly lower than the original precursor membrane before the sulfonating treatment (Figure S4b), but the

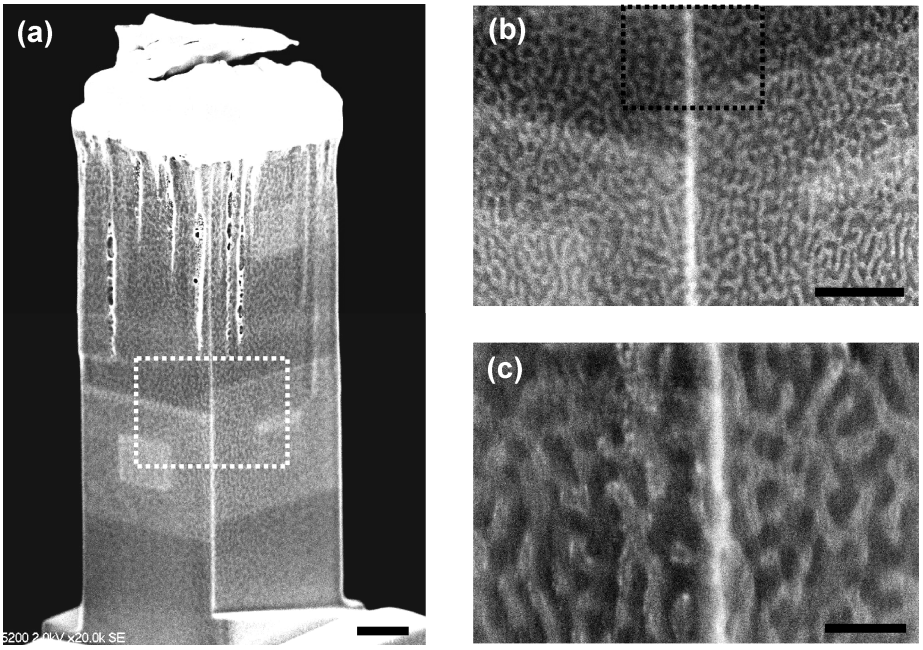

Figure 3. Grazing SEM images of a membrane sulfonated under the optimum conditions. (a) Entire image with a scale bar of 1 μm. (b, c) Enlarged images of the areas marked by the dotted white and black squares in (a) and (b), with scale bars of 500 and 150 nm.

melting peak temperature increased over 100 °C after sulfonation. When the weight change caused by sulfonation was taken into account, these fusion heats recorded before and after sulfonation were almost the same. This also supports the selective sulfonation of PS components while retaining the crystalline PE components. The increase in melting peak temperature can be explained by pairing sulfonic acid groups in the molten state, which reduces the entropy in the molten state.[29] Actual fuel-cell application requires thermal stability up to 80 °C.[30]

Indeed, various polymer electrolyte membranes have been prepared from BCP,[31−38] but the reported water uptakes are higher than that obtained in this study under the same measurement conditions. This remarkable difference stems from the highly crystalline state of the hydrophobic phase in this study, which is still maintained after sulfonating treatment, as discussed above. Nafion membranes also exhibit less melting endotherm, indicating an amorphous backbone structure.

The mechanical properties of our electrolyte membrane were compared to a commercial Nafion membrane (Figure S5). The stress−strain curves were recorded at room temperature in the dried state for both membranes. The tensile strength and modulus of our membrane were 15 and 127 MPa, which are both halves the Nafion membrane. Ideal thermal and mechanical properties are to be expected from an alternative backbone structure tougher than a combination of PE and PSS, but this exceeds the purpose of this study, i.e., the proposal of a unique design solving the conductivity vs water-uptake trade-off for polymer electrolyte membrane.

The reliability of the electrolyte properties was verified by repeating the swelling/drying procedures made after the first test (Table 1). The values in the second run were obtained after the membrane was again immersed in deionized water at room temperature for 24 h, and its weight was measured for water uptake in the second run. This swollen membrane was placed in with an electrolyte cell (Figure S3) and equilibrated at 50 °C and 90% humidity for 1 h, followed by ac impedance recording. The membrane was then dried at 40 °C for 10 h for weight measurement in the dried state. A third run was also carried out after the same membrane was immersed in deionized water for 24 h at room temperature and dried at 40 °C for 7 h. It should be noted that a thermal gravimetry analysis (TGA) indicated that the residual water content within the dried membrane before the second run was 0.1 wt %, which was evaluated as the weight loss at 100 °C (Figure S6). This value was the same level as that for the dried Nafion membrane (0.2 wt %). The second run produced electrolyte properties similar to those for the first run. Similarly, few changes were recognized in the third run. This means that repeating the swelling/drying procedures could destroy the crystalline network structure initially formed from the bicontinuous phase arrangement of the precursory BCP morphology, decreasing the proton conductivity and increasing the water uptake. However, it should be noted that the obtained water uptake for the third run was still lower than that of Nafion.

In order to discuss the origin of the lower water uptake for the electrolyte membrane developed in this study, we calculated the number of water molecules trapped per sulfonic acid. Here, full sulfonation of the PS components was assumed, as confirmed in Table 1. The membranes prepared in this study had one or two molecules per sulfonic acid in the resultant PSS component. This is one-fifth of the 10−20 molecules estimated for the Nafion membrane.[8,39] Two different proton-transport mechanisms have been suggested: proton "hopping" (Grotthus), where protons hop from one hydrolyzed ionic site ($SO_3^-H_3O^+$) to another across the membrane, and electroosmotic drag, where protons bound to water ($H^+(H_2O)_x$) drag one or more water molecules across the membrane.[6] The former mechanism requires one water molecule per sulfonic acid for effective proton transport, which coincides with our estimation in Table 1. The latter mechanism is associated with the forming and breaking of hydrogen bonds in the neighborhood of the proton position, corresponding to Eigen ($H_9O_4^+$) or Zundel ions ($H_5O_2^+$), which are considered to be the origin of anomalously high proton mobility in free water.[40] Indeed, *ab initio* calculations for the Nafion membrane also suggested that at least three water molecules per sulfonic acid are required for proton dissociation.[41] However, these models incorporate the ability of the proton to undergo a Grotthus-like hopping by which one H_3O^+ ion is transferred to a neighboring water molecule.[42] This proton-transport mechanism seems to be characteristic of the unique hydrophilic-channel networks constrained by hydrophobic-backbone networks obtained in this study, giving

a lower water uptake. A more detailed discussion on the proton-transport mechanism for our electrolyte membrane structure will be provided in a future study by proton-diffusion measurements using solid-state NMR techniques.

These estimates indicate to us that our electrolyte membrane forms continuous proton-conductive channels of the PPS component with less volume expansion, which is identical even in the initial dried state. This insight was confirmed by internal morphological analyses by grazing scanning electron microscopy (SEM) after sulfonation. Figure 3 presents a series of 3-D images for the sulfonated membrane listed in the first column in Table 1. The membrane was treated by RuO_4 vapor that selectively stains the PPS components, and a square pole was cut out by a focused gallium ion beam (FIB) procedure in the SEM chamber. The membrane surface was coated by tungsten ion sputtering, which appears as a bright layer on the top of the pole (Figure 3a). The holes under this tungsten coating are marked during an FIB procedure. As seen in Figure 3a, sufficient contrast is obtained even at the foot of the pole, corresponding to a 10 μm depth from the outer surface of the membrane. For a typical dense PE film with no pores, RuO_4 vapor permeates to less than a 1 μm depth from the sample surface;[43] thus, the deep staining in Figure 3a indicates that stainable PPS channel networks are homogeneously spread over the whole region of the membrane.

Here, bright (dark) regions within the internal structure correspond to the crystalline PE backbone (amorphous PSS matrix). In the enlarged images in Figure 3b,c, both sides of the observed sections exhibit bicontinuous arrangements of stained PSS channels and PE crystalline backbones, which is similar to the initial morphology of the PE-*b*-PS film before sulfonating treatment (Figure 1). The diameter of the backbone PE cylinders was 30 nm in both cases. These structural similarities demonstrate that bicontinuous crystalline/amorphous phase arrangements initially formed by isothermal crystallization procedures can be maintained even after sulfonating treatment, which is coincident with the results of solid-state NMR (Figure 2). The corresponding morphology can be observed over the whole region of the pole, indicating homogeneous spreading of PSS channel networks and PE crystalline backbones within the whole membrane size of 20 mm $\times$ 50 mm $\times$ 30 μm.

In summary, a combination of proton conductive and solid backbone networks can be prepared from bicontinuous crystalline/amorphous phases of a BCP precursor. Such phase connections can be maintained even when membrane swelling and drying were repeated. As described above, the unique introduction of a crystalline component in the electrolyte membrane resulted in structural stability in the proton conductive channels, which is a key to the desirable electrolyte properties obtained in this study.

Acknowledgment. We thank Dr. Kazuhiro Aoyama (FEI Company Japan Ltd.) for 3-D TEM imaging using an FEI Tecnai G2 F20.

Supporting Information Available: Table S1, Figures S1−S6, and a description of the experimental procedures. This material is available free of charge via the Internet at http://pubs.acs.org.

References and Notes

(1) Dusastre, V. *Nature* **2001**, *414*, 331.
(2) Schultz, M. G.; Diehl, T.; Brasseur, G. P.; Zittel, W. *Science* **2003**, *302*, 624.
(3) Jacobson, M. Z.; Colella, W. G.; Golden, D. M. *Science* **2005**, *308*, 1901.
(4) Rikukawa, M.; Sanui, K. *Prog. Polym. Sci.* **2000**, *25*, 1463.
(5) Hickner, M. A.; Ghassemi, H.; Kim, Y. S.; Einsla, B. R.; McGrath, J. E. *Chem. Rev.* **2004**, *104*, 4587.
(6) Deluca, N. W.; Elabd, Y. A. *J. Polym. Sci., Polym. Phys. Ed.* **2006**, *44*, 2201.
(7) Nasef, M. M.; Hegazy, E.-S. A. *Prog. Polym. Sci.* **2006**, *29*, 499.
(8) Mauritz, K. A.; Moore, R. B. *Chem. Rev.* **2004**, *104*, 4535.
(9) Kim, M.-H.; Glinka, C. J.; Grot, S. A.; Grot, W. G. *Macromolecules* **2006**, *39*, 4775.
(10) Schmidt-Rohr, K.; Chen, Q. *Nat. Mater.* **2008**, *7*, 75.
(11) Majsztrik, P.; Bocarsly, A.; Benziger, J. *J. Phys. Chem. B* **2008**, *112*, 16280.
(12) Spry, D. B.; Goun, A.; Glusac, K.; Moilanen, D. E.; Fayer, M. D. *J. Am. Chem. Soc.* **2007**, *129*, 8122.
(13) Park, C.; Yoon, J.; Thomas, E. L. *Polymer* **2003**, *44*, 6725.
(14) Olson, D. A.; Chen, L.; Hillmyer, M. A. *Chem. Mater.* **2008**, *20*, 869.
(15) De Rosa, C.; Park, C.; Thomas, E. L. *Nature* **2000**, *405*, 433.
(16) Lorenzo, A. T.; Arnal, M. L.; Müller, A. J.; Boschetti-de-Fierro, A.; Abetz, V. *Eur. Polym. J.* **2006**, *42*, 516.
(17) Lorenzo, A. T.; Arnal, M. L.; Müller, A. J.; Boschetti-de-Fierro, A.; Abetz, V. *Macromolecules* **2007**, *40*, 5023.
(18) Müller, A. J.; Castillo, R. V.; Hillmyer, M. A. *Macromol. Symp.* **2006**, *242*, 174.
(19) Wang, Y.; Hillmyer, M. A. *J. Polym. Sci., Polym. Chem. Ed.* **2001**, *39*, 2755.
(20) Myers, B. S.; Register, R. A. *Macromolecules* **2008**, *41*, 6773.
(21) Jones, B. H.; Lodge, T. P. *J. Am. Chem. Soc.* **2009**, *131*, 1676.
(22) Uehara, H.; Yoshida, T.; Kakiage, M.; Yamanobe, T.; Komoto, T.; Nomura, K.; Nakajima, K.; Matsuda, M. *Macromolecules* **2006**, *39*, 3971.
(23) Uehara, H.; Yoshida, T.; Kakiage, M.; Yamanobe, T.; Komoto, T. *J. Polym. Sci., Polym. Phys. Ed.* **2006**, *44*, 1731.
(24) Uehara, H.; Kakiage, M.; Sekiya, M.; Yamanobe, T.; Takano, N.; Barraud, A.; Meurville, E.; Ryser, P. *ACS Nano* **2009**, *3*, 924.
(25) Gübler, L.; Gursel, S. A.; Scherer, G. G. *Fuel Cells* **2005**, *5*, 317.
(26) Xu, T.; Woo, J.-J.; Seo, S.-J.; Moon, S.-H. *J. Membr. Sci.* **2008**, *325*, 209.
(27) Yamanobe, T.; Ando, I. *J. Chem. Phys.* **1985**, *83*, 3154.
(28) Yamanobe, T.; Sorita, T.; Komoto, T.; Ando, I.; Sato, H. *J. Mol. Struct.* **1985**, *131*, 267.
(29) Okui, N.; Narita, N.; Shimada, T.; Kawai, T. *Kobunshi Ronbunshu* **1974**, *31*, 469.
(30) Kim, D. S.; Kim, Y. S.; Guiver, M. D.; Ding, J.; Pivovar, B. S. *J. Power Sources* **2008**, *182*, 100.
(31) Tsang, E. M. W.; Zhang, Z.; Shi, Z.; Soboleva, T.; Holdcroft, S. *J. Am. Chem. Soc.* **2007**, *129*, 15106.
(32) Siu, A.; Schmeisser, J.; Holdcroft, S. *J. Phys. Chem. B* **2006**, *110*, 6072.
(33) Ghassemi, H.; McGrath, J. E.; Zawodzinski, T. A.Jr. *Polymer* **2006**, *47*, 4132.
(34) Ghassemi, H.; Ndip, G.; McGrath, J. E. *Polymer* **2004**, *45*, 5855.
(35) Roy, A.; Yu, X.; Dunn, S.; McGrath, J. E. *J. Membr. Sci.* **2008**, *327*, 118.
(36) Lee, C. H.; Lee, S. Y.; Lee, Y. M.; Lee, S. Y.; Rhim, J. W.; Lane, O.; McGrath, J. E. *ACS Appl. Mater. Interfaces* **2009**, *1*, 1113.
(37) Norsten, T. B.; Guiver, M. D.; Murphy, J.; Astill, T.; Navessin, T.; Holdcroft, S.; Frankamp, B. L.; Rotello, V. M.; Ding, J. *Adv. Funct. Mater.* **2006**, *16*, 1814.
(38) Nieh, M.-P.; Guiver, M. D.; Kim, D. S.; Ding, J.; Norsten, T. *Macromolecules* **2008**, *41*, 6176.
(39) Cui, S.; Liu, J.; Selvan, M. E.; Paddison, S. J.; Keffer, D. J.; Edwards, B. J. *J. Phys. Chem. B* **2008**, *112*, 13273.
(40) Marx, D.; Tuckerman, M. E.; Hutter, J.; Parinello, M. *Nature* **1999**, *397*, 601.
(41) Paddison, S. J. *J. New Mater. Electrochem. Syst.* **2001**, *4*, 197.
(42) Spohr, E.; Commer, P.; Kornyshev, A. A. *J. Phys. Chem. B* **2002**, *106*, 10560.
(43) Trent, J. S.; Scheinbeim, J. I.; Couchman, P. R. *Macromolecules* **1983**, *16*, 589.